IEEE Access
Multidisciplinary | Rapid Review | Open Access Journal

Received April 16, 2021, accepted May 2, 2021, date of publication May 7, 2021, date of current version May 18, 2021.

Digital Object Identifier 10.1109/ACCESS.2021.3078163

A Novel Erbium-Doped Fiber Laser Chaotic Circuit Based on Memristor and Its Circuit Implementation

JIEYANG WANG, HONGJIE LI, ZHISEN WANG, AND JUN MOU
School of Information Science and Engineering, Dalian Polytechnic University, Dalian 116034, China

Corresponding author: Hongjie Li (lihj@dlpu.edu.cn)

This work was supported in part by the National Natural Science Foundation of China under Grant 62061014, and in part by the Natural Science Foundation of Liaoning Province under Grant 2020-MS-274.

ABSTRACT In this paper, a new chaotic system is proposed by adding a magnetron memristor to an erbium-doped fiber laser circuit, and its dynamical characteristics are analyzed. A special periodic coexistence attractor phenomenon was discovered during the analysis, which affects the dynamical characteristics of the system by changing the time parameters of the AC power supply and it is controllable. Finally, the chaotic system is implemented by constructing an equivalent analog circuit. Theoretical analysis and simulation results show that the new erbium-doped fiber laser chaotic system has good dynamical characteristics and it is easy to implement. Meanwhile, the rich dynamical characteristics of the system provide a basis for its application in image encryption and other fields.

INDEX TERMS Single-ring, erbium-doped fiber laser, memristor, coexistence of periodic attractors, analog circuit implementation.

I. INTRODUCTION

In 1985, Lorenz laser chaos of Haken model was discovered and verified by Weiso et al in the NH3 lasers system [1]. After that, many laser chaotic characteristics of the Haken model was verified in far infrared lasers [2], [3]. In the same year, from studying the Xe lasers system with the non-uniformly widened model, Casperson observed the self-pulsation of the laser, which is caused by membrane splitting instability and can be described by the Maxwell Schrodinger semi-classical equation. The reason for this phenomenon is the crossover relaxation effect, which is caused by the direct spontaneous relaxation effect and rate variation between two energy levels [4]. In the He-Ne laser, Abraham *et al.* changed the degree of non-uniform widening by changing the partial pressure of the Ne gas and observed the laser film split, self-pulsation oscillation, and chaos. In the most laser systems, the phenomenon of entering chaos through period-doubling bifurcated channel, quasi-periodic channel and intermittent chaotic channel has been observed [5]. Compared with the traditional circuit chaotic system, the laser chaotic systems usually has larger bandwidth, lower attenuation, more complex dynamical behaviors, and greater sensitivity to parameter variations, so it can be widely used in high speed remote confidential communications [6]–[8].

As the representative of the third generation of lasers, fiber lasers doped with rare earth elements are more suitable for laser chaos research due to their low cost, low threshold, and high electro-optical efficiency [9], [10]. Compared with other fiber lasers, the loss coefficient of erbium-doped fiber laser (EDFL) is lower and is only 0.2dB/km. EDFL has excellent characteristics such as high gain, good noise characteristics, and polarization insensitivity [11]–[13]. EDFL's dielectric material erbium-doped fiber has several characteristics such as high metastable life, the high power density of the fiber core, and high gain, benefit from this, EDFL is suitable for using in military security communications and optical communications [14]–[16]. The rate equation of EDFL is a second-order dynamical system, determined by its laser field intensity and the number of inverted particles, so the system of EDFL cannot enter chaos spontaneously [17]. The main means to improve the laser into a chaos laser are modulation parameters, increasing the number of modes, and injecting external fields [18]. By changing the rate equation parameters and adding degrees of freedom, the EDFL system can be improved into a chaotic dynamical system [19]–[21].

The associate editor coordinating the review of this manuscript and approving it for publication was Sun Junwei.

The traditional method of constructing laser chaos has limitations and cannot realize the diversification of system characteristics. These disadvantages are detrimental to military applications and laser confidential transmission. Therefore, it is necessary to propose a method that can realize the diversification of laser chaos and make its structure and dynamical characteristics more complicated [22], [23].

In 1971, Leon O. Chua predicted the existence of memristors from the perspective of circuit theory completeness [24]. Memristor is a passive basic circuit element that describes the relationship between magnetic flux and charge in addition to resistance, capacitance and inductance [25], [26]. As the fourth passive element, memristor has the advantages of high speed, low power consumption, easy integration, and simple structure [27]–[29]. Memristor is a special nonlinear resistor with charge memory function, which can realize 0-1 information storage function [30]. It becomes the core basic element of the Nonvon Neumann computer architecture for information storage and fusion computing in the future [31], [32]. Nonlinear element memristor is introduced into the EDFL system to add degrees of freedom to the EDFL rate equation [33]. In dynamical analysis, ideal memristor circuit model derived from the actual memristor is often used [34].

A new method of putting the memristor into the laser system is introduced, by this method, EDFL system becomes a new nonlinear system which can produce chaos [35]. The memristor laser chaotic system which can be obtained by this method is different from the ordinary laser chaotic system, the equilibrium points of system are a set of points on a line, and the dynamical characteristics are more complex [36]. EDFL is expensive and complex, and the resonant cavity of it is a linear cavity [37], [38]. In this kind of resonant cavity, the cavity mirror is in close contact with the end face of the optical fiber, and the cavity mirror is perpendicular to the axis of the optical fiber [39]. With this structure, the cavity mirror and the fiber end face are coupled with high precision to avoid loss due to beam divergence [40]. Therefore, a slight tilt in the end face of the fiber or the cavity mirror will rapidly increase the loss of the laser [41]. Besides, in the resonant cavity, the end reflector is sensitive to the smoothness of the fiber end face, and subtle defects can cause damage to the instrument [42], [43]. Therefore, the memristors cannot be introduced into the laser system during the theoretical analysis period. Using a simulation model instead of EDFL for simulation experiments, a method of constructing a simulation circuit for verification is simple and accurate [44]–[46]. The simulation circuit can show the same dynamical characteristics as the laser chaos system, and its structure is simple, which is more suitable for studying the dynamical characteristics of EDFL [47], [48]. In military secure communication and optical communication, memristor laser chaotic systems have excellent application value. This method of constructing a chaotic system combines the memristor with the laser system, which provides a new idea for the study of the field of laser chaotic system [49]–[51].

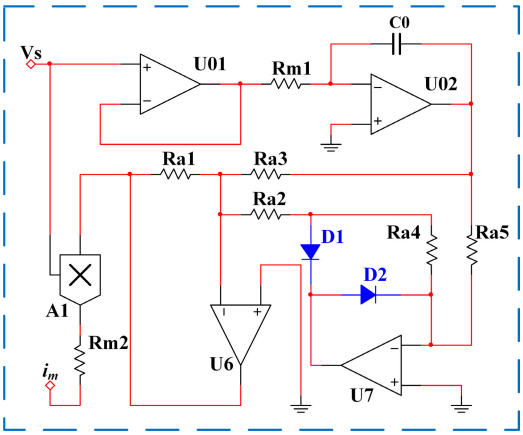

FIGURE 1. Circuit diagram of the absolute value memristor.

The structure of this paper is described below. The section 2 gives the memristor model and its volt-ampere characteristics analysis. In the section 3, the proposed laser chaotic system is given, and its dynamical characteristics are analyzed. In the section 4, a practical analog circuit is built and used to verify the results of theoretical analysis. In the section 5, the content of this paper is summarized.

II. MODEL OF THE MEMRISTOR

A magnetron memristor was proposed by Bao *et al.* in reference [52], [53], this memristor can be described by a smooth quadratic nonlinear characteristic curve. In this section, the magnetron memristor is improved, and the non-linear part is replaced by the absolute value function circuit, making it a new absolute value memristor. The circuit schematic is shown in Fig. 1, and the mathematical theoretical model of memristor can be expressed as Eq. 1.

$$\begin{cases} i = W(\varphi)v \\ \dfrac{d\varphi}{dt} = v \\ W(\varphi) = -a + b\,|\varphi| \end{cases} \tag{1}$$

the volt-ampere relationship between voltage and current are

$$\begin{cases} i_m = W(\varphi)v_s \\ \dot{\varphi} = v_s \end{cases} \tag{2}$$

the function image of Eq. (1) is a characteristic curve through the origin. The slope of the curve is called the memductance, which represents the proportional relationship between the number of charges and the magnetic flux, the unit of memductance and conductance are both Siemens. Where vs is AC power and can be expressed as $vs = A\sin(2\pi ft)$, A of $vs$is the amplitude of the AC power source, and f is the frequency of the AC power source. $W(\varphi)$ is a continuous function of φ.

$$W(\varphi) = \alpha + \beta\,|\varphi| \tag{3}$$

where α and β are the coefficients of the memristor, φ is the magnetic flux of the memristor. A sinusoidal AC voltage

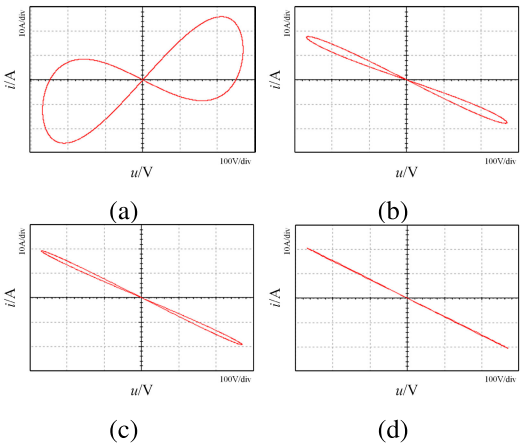

FIGURE 2. The volt-ampere characteristic curve of the memristor at different frequencies of *vs*, (a) $f = 5$ Hz, (b) $f = 50$ Hz, (c) $f = 100$ Hz, (d) $f = 1000$ Hz.

source vs is connected to the input of the memristor proposed in Eq. (1), where $\alpha = 0$ and $\beta = 1$. When keeping $A = 19$V and assigning the frequency f to 5 Hz, 50 Hz, 100 Hz, 1000 Hz, respectively. The component value is selected as $Rm_1 = 50\text{k}\Omega$, $Rm_2 = 1\text{k}\Omega$, $Ra_1 = 10\text{k}\Omega$, $Ra_2 = 5\text{k}\Omega$, $Ra_3 = 10\text{k}\Omega$, $Ra_4 = 10\text{k}\Omega$, $Ra_5 = 10\text{k}\Omega$, and $g_1 = 1$, the volt-ampere characteristics of memristor are shown in Fig.2. The volt-ampere relationship diagram of the memristor is a close hysteresis loop through the origin when using sinusoidal AC excitation. As the frequency f increases, the hysteresis side-lobe area gradually decreases, until the frequency increases to 1000Hz, the volt-ampere relationship becomes a straight line across the origin. This is consistent with the essential characteristics of memristors.

III. SINGLE-RING ERBIUM-DOPED FIBER LASER CHAOTIC SYSTEM BASED ON MEMRISTOR

A. LASER CHAOS SYSTEM

The model of the single-ring erbium-doped fiber laser is described by two first-order ordinary differential equations as

$$\begin{cases} \dfrac{dE}{dt} = -kE + gED \\ \dfrac{dD}{dt} = -[I_p + 1 + |E|^2]D + I_p - 1 \end{cases} \tag{4}$$

where E is the output light intensity of the laser, k and g are the loss coefficient and gain coefficient of the laser respectively, D is the number of population inversion, and Ip is the pump light intensity. Let $E = x$, $D = y$, $k = a$, $g = b$, $Ip = c$, and the dimensionless equation obtained by normalization calculation is

$$\begin{cases} \dot{x} = -ax + bxy \\ \dot{y} = -(1 + c + x^2)y + c - 1 \end{cases} \tag{5}$$

when the system parameters are $a = 1000$, $b = 4600$, $Ip = 4.0$, the initial value is (13.5, 0.1), and the step size is 0.001s, the Lyapunov exponent of the system is (−6.8958, −6.9063), and the attractor is shown in Fig. 3.

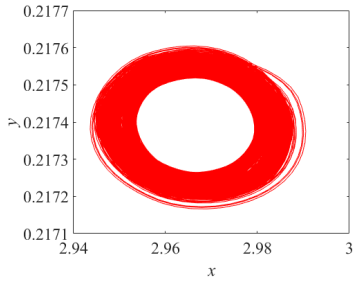

FIGURE 3. The *x-y* plane phase diagram of the EDFL system, when the system parameters are $a = 1000$, $b = 4600$, $Ip = 4.0$, the initial value is (13.5, 0.1), and the step length is 0.001.

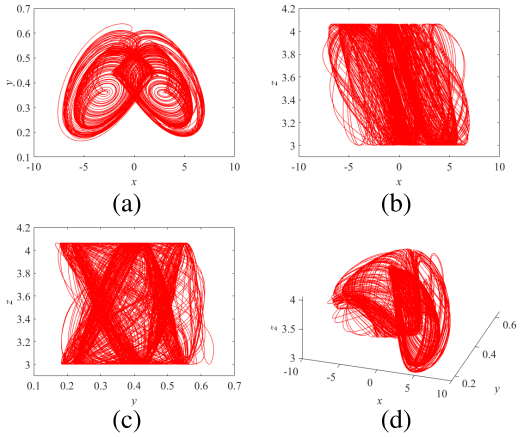

FIGURE 4. The phase diagram of the new system, when the parameters are $a = 55$, $b = 167$, $c = 6.9$, $A = 19$, $f = 5.7$, and the initial value is (10, 0, 3), (a) *x-y* plane, (b) *x-z* plane; (c) *y-z* plane, (d) phase diagram of *x-y-z* in three dimensions.

By using the modulation method to add a degree of freedom to the erbium-doped fiber laser, that is, adding a magnetron ideal memristor to the first equation in Eq. (5), a third-order memristor laser system is proposed. The dimensionless equation is expressed as

$$\begin{cases} \dot{x} = -ax + bxy - W(z)v_s \\ \dot{y} = -(1 + c + x^2)y + c - 1 \\ \dot{z} = v_s \end{cases} \tag{6}$$

The new variable z represents the magnetic flux φ, that is $W(z) = |z|$, the sinusoidal AC power is $vs = A\sin(2\pi ft)$, and $W(z)vs$ represents the light field intensity of the Coherent Field. When the new system parameters are $a = 55$, $b = 167$, $c = 6.9$, $A = 19$, $f = 5.7$, the initial value is (10, 0, 3), the time step is 0.001s. At this point, the Lyapunov exponent of the new system is (2.1579, 0, −9.7596), and the fractal dimension of the system is 2.2211, the simulation results show that the system is chaotic. The phase diagram and time-domain diagram are shown in Fig. 4 and Fig. 5 at this time.

In order to study more dynamical characteristics about the new system, 15 attractors with different parameter values are selected. When the initial value is (10, 0, 3) and the step size is 0.001s, the system phase diagram is shown in Fig. 6, and

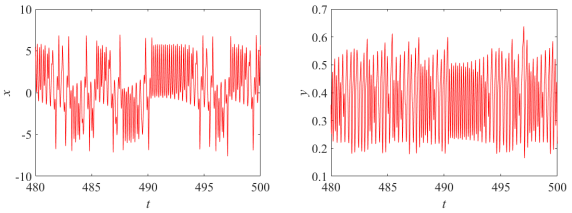

FIGURE 5. The time-domain diagram of the new system, when the parameters are $a = 55$, $b = 167$, $c = 6.9$, $A = 19$, $f = 5.7$, and the initial value is (10, 0, 3), (a) t-x plane, (b) t-y plane.

the relationship between the attractor, Lyapunov exponents, and fractal dimension is shown in Table 1.

B. EQUILIBRIUM POINT SET AND STABILITY

It can be concluded that the divergence of system (6) is

$$\nabla V = \frac{\partial \dot{x}}{\partial x} + \frac{\partial \dot{y}}{\partial y} + \frac{\partial \dot{z}}{\partial z} = -a + by - 1 - c - x^2 \tag{7}$$

the parameters were selected as $a = 55$, $b = 167$, $c = 6.9$, $A = 19$, $f = 5.7$,, the initial value is (10, 0, 3), and Eq. (7) less than zero.

By solving the equations system $\dot{x} = \dot{y} = \dot{z} = 0$, which lead to -$ax + bxy$-$|z|vs = 0$, $-(1 + c + x^2)y + c$-$1 = 0$ and $vs = 0$. Because the system is a non-autonomous system, the stability of the system can be changed by changing the time parameter t of the ideal voltage source. When the time parameter t makes $A\sin(2\pi ft) = 0$, the system is unfolded, so the attractor that appears in this state is hidden. When the time parameter t makes $A\sin(2\pi ft) = 0$, the system is obtained. The result is obtained as $x_1 = \pm 5.0808i$, $y_1 = 0.3293$, $x_2 = 0$, $y_2 = 0.7468$. Since x_1 is a complex number, the point (x_1, y_1) does not conform to the property of the equilibrium point and be discard, the equilibrium point set is obtained as P(0, 0.7468, n), where n is any real number. Linearizing Eq. (6) at the equilibrium point set P, the Jacobian matrix can be obtained as

$$J = \begin{bmatrix} by - a & bx & -sgn(z)v_s \\ -2xy & -x^2 - c - 1 & 0 \\ 0 & 0 & 0 \end{bmatrix} \tag{8}$$

the characteristic polynomial of Jacobian matrix J is

$$f(\lambda) = A_3\lambda^3 + A_2\lambda^2 + A_1\lambda + A_0 \tag{9}$$

where $A_3 = -1$, $A_2 = (by - a - g - 1\text{-}x^2)$, $A_1 = (by - ag - a - ax^2 - bx^2y + bgy)$ and $A_0 = 0$. According to the Routh-Hurwitz criterion, the equilibrium point is stable, when $A_i > 0$, $(i = 1, 2, 3)$; $A_2A_1 > A_3A_0$. According to the analysis of the Jacobian matrix, it can be seen that different values of n will not change the characteristic polynomial and eigenvalues of the Jacobian matrix. Since $A_3 = -1 < 0$, $\lambda_3 > 0$, all of the balance points in the Points set P are unstable.

C. THE IMPACTS OF PARAMETERS

The system parameters are selected as $a = 55$, $b = 167$, $c = 6.9$, $A = 19$, initial value is set to (10, 0, 3), simulation step is set to 0.01s. Lyapunov exponents and bifurcation diagram with parameter f are shown in Fig. 7 when the system parameter f gradually increases from 5 to 6.

When $5 < f < 5.572$, system maintains a periodic state; When $f = 5.573$, the Lyapunov exponent of system is (0.4580, 0, -8.9836), and system enters chaotic state from this point. When f$\in$(5.72, 5.727), there are several discontinuous points in the periodic state of the system, and the periodic window displayed on the bifurcation diagram is too small to be detected. When $f = 5.839$, the Lyapunov exponent of system is (0, -0.1232, -9.5953). From this value, the system gradually breaks out of chaos and returns to a periodic state.

keeping other parameters constant, $f = 5.7$, and selecting the system parameter c gradually increases from 5 to 8. The Lyapunov exponents and bifurcation diagram are shown in Fig. 8. When $c < 5.94$, system maintains a periodic state, and if $5.95 < c < 7.14$, system enters chaos with intermittent chaos. When $c = 5.95$, the Lyapunov exponent of system is (0.7916, 0, -5.6370), and system enters chaos. When $6.76 < c < 6.79$, the system is in the periodic window, when $c = 6.76$, the Lyapunov exponent of the system is (0, -1.1590, -9.6175), the Lyapunov exponent is (0, -1.2122, -9.8033) when $c = 6.79$. When $c > 7.15$, the system starts to enter the periodic state, and the Lyapunov exponent is (0, -0.5881, -8.5842).

D. COEXISTENCE OF ATTRACTORS

1) SYMMETRIC ATTRACTOR COEXISTENCE

When system parameters are constant and different initial conditions are selected, system produce different attractors, this phenomenon is called attractor coexistence. The coexistence of attractors with multiple stable states is a special phenomenon in nonlinear systems. A few nonlinear systems can even produce an infinite number of coexisting attractors [54], [55]. It is usually called extremely multi-stability, and it has great application value.

When the new system parameters are $a = 55$, $b = 167$, $c = 6.9$, $A = 19$, $f = 5.7$, the initial value is selected (10, 0, x), where x is variable in the initial value, recording the changes of the system attractors. Under this conditions, the new system undergoes a "period-chaos-period-chaos-period" conversion process as the initial value x increases. The new system takes x = -0.5 as the central axis, and the phase diagrams on both sides of the central axis are symmetrical. When $x > 6$ or $x < -8$, the phase diagram no longer changes with the increase of the absolute value of x. The attractors for $x \in (-8, 7)$ are shown in Fig. 9.

2) PERIODIC ATTRACTOR COEXISTENCE

When studying the coexistence of symmetry attractors in section 3.4.1, if the parameters are $a = 55$, $b = 167$, $c = 6.9$, $A = 19$, $f = 5.7$ and the initial value is (10, 0, 3), the time

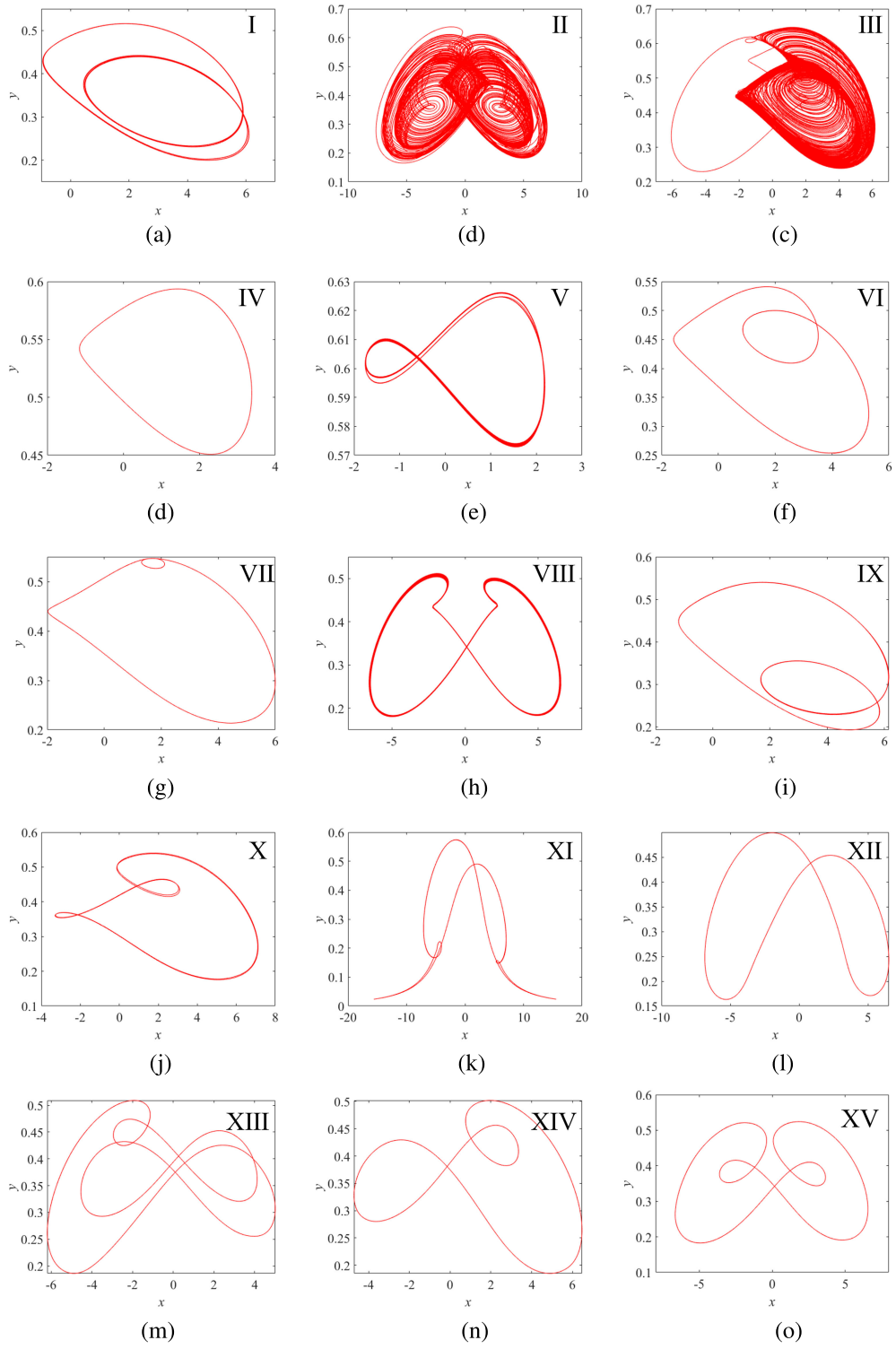

FIGURE 6. Phase attractors of the x-y plane with different parameters, when the initial value is (10, 0, 3), (a) $a = 51$, (b) $a = 55$, (c) $a = 67$, (d) $a = 84$, (e) $a = 98$, (f) $b = 142$, (g) $b = 149$, (h) $b = 172$, (i) $b = 194$, (j) $A = 26$, (k) $f = 0.1$, (l) $f = 1.8$, (m) $f = 3.9$, (n) $f = 4.3$, (o) $f = 4.8$.

constant t of the AC voltage source was designed to be a variable. Under this condition, a new attractor coexistence phenomenon was discovered in the new system, and this coexistence attractor is periodic and sequential.

The initial condition t is set as a variable and the attractors of the new system are observed. The attractor coexistence of the new system produces a special form. When the value of t increases from $+\infty$ to $-\infty$ successively, the attractor appears

TABLE 1. The value and unit of the components in Fig. 6.

Serial number	a	b	A	f	Lyapunov exponent	Fractal dimension
I	51	167	19	5.7	(0, -0.3212, -10.6587)	1
II	55	167	19	5.7	(2.1579, 0, -9.7596)	2.2211
III	67	167	19	5.7	(1.0197, 0, -6.5986)	2.1545
IV	84	167	19	5.7	(0, -3.8058, -3.8002)	1
V	98	167	19	5.7	(0, -1.9450, -5.6794)	1
VI	55	142	19	5.7	(0, -0.3234, -9.6859)	1
VII	55	149	19	5.7	(0, -3.0154, -3.0765)	1
VIII	55	172	19	5.7	(0, -3.1151, -7.0486)	1
IX	55	194	19	5.7	(0, -1.6300, -5.8088)	1
X	55	167	26	5.7	(0, -2.7831, -5.4753)	1
XI	55	167	19	0.1	(0, -1.0915, -183.9896)	1
XII	55	167	19	1.8	(0, -5.0469, -21.3153)	1
XIII	55	167	19	3.9	(0, -1.4134, -9.1886)	1
XIV	55	167	19	4.3	(0, -5.8879, -5.8856)	1
XV	55	167	19	4.8	(0, -1.2883, -7.1098)	1

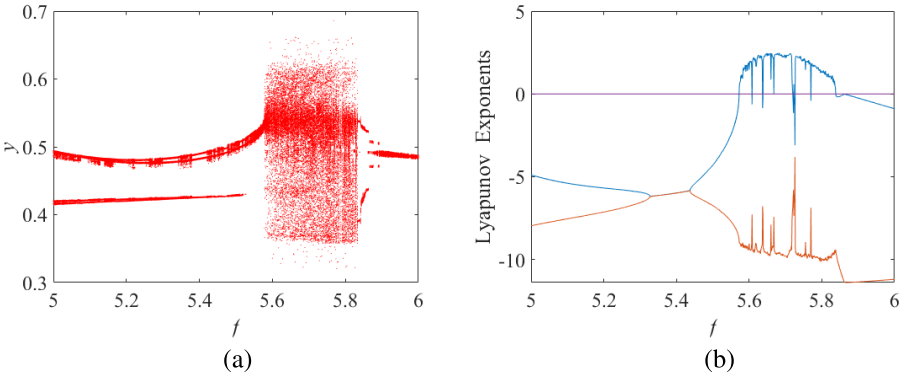

FIGURE 7. Lyapunov exponent spectrum and bifurcation diagram with parameter *f*. (a) bifurcation diagram, (b) Lyapunov exponent spectrum.

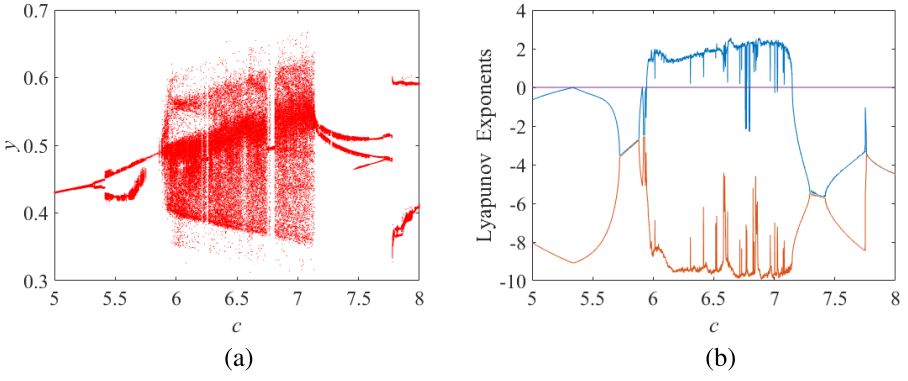

FIGURE 8. Lyapunov exponent spectrum and bifurcation diagram with the initial conditions (10, 0, 3), the parameters $a = 55$, $b = 167$, $A = 19$, $f = 5.7$, and the variation of circuit parameter c, (a) bifurcation diagram, (b) Lyapunov exponent spectrum.

obvious periodicity. The phase diagram of the new system when we choose $t \in (4, 18)$ is shown in Fig. 10.

From the Fig. 10, it can be found that when $t = 4$ and $t = 14$, $t = 5$ and $t = 15$, $t = 6$ and $t = 16$, $t = 7$ and $t = 17$, and $t = 8$ and $t = 18$, the system phase diagrams show same shape and size, respectively. Since the time variable t directly affects the value of the AC power supply, a hypothesis is proposed, the coexistence of periodic attractors is related to

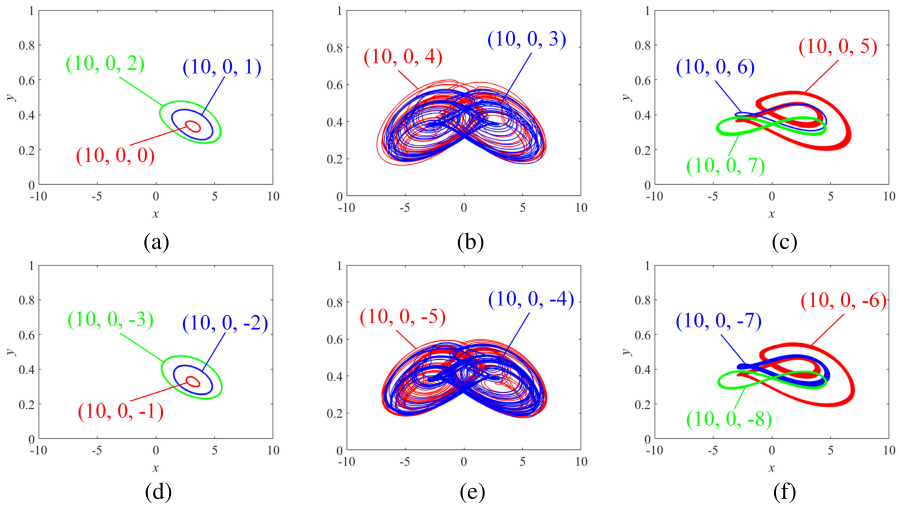

FIGURE 9. The x-y plane phase diagram when the new system parameters are $a = 55$, $b = 167$, $c = 6.9$, $A = 19$, $f = 5.7$, (a) (10, 0, 0), (10, 0, 1) and (10, 0, 2), (b) (10, 0, 3) and (10, 0, 4), (c) (10, 0, 5), (10, 0, 6) and (10, 0, 7), (d) (10, 0, −1), (10, 0, −2) and (10, 0, −3), (e) (10, 0, −4) and (10, 0, −5), (f) (10, 0, −6), (10, 0, −7) and (10, 0, −8).

the result of the function $s = \sin(x)$. According to this assumption, simulating the phase diagram of the system under the condition of different time parameter t values and calculated the value of the function $s = \sin(x)$, and the results are shown in Table 2.

According to the analysis of the data in the Table 2, the result of $s = \sin(x)$ has strong regularity. The system will enter chaotic state every few t-values, and the system will repeat the previous state every 10 t-values. The function image was made from the experimental data from Table 2, and the position of the chaotic state is marked in the image, as shown in Fig. 11.

When $t = -3$, $t = 0$, $t = 3$ and $t = 7$, the system enters chaos, and the results of $s = \sin(t)$ are $s = -0.5878$, $s = 0$, $s = 0.5878$ and $s = -0.5878$ respectively. By comparing with Table 2, the system will not enter chaos when $s = \sin(x) = \pm 0.9511$. So, the state of the system can be determined by the value of the sine function, when the initial condition t is an integer.

When $t \in (3, 7)$, a more detailed analysis was conducted, selecting a t value every 0.1-time unit, and observing the process of the new system state change. There is a chaotic state between the two chaotic states when the time parameter t takes the score value. At the same time, the result of $s = \sin(x)$ is recorded and analyzed, as shown in Table 3.

To explore in-depth, the time parameter $t \in (4.91, 5.82)$ is selected for analysis, taking a position every 0.01-time unit, the types of attractors increased. When analyzing two adjacent same type attractors, no new attractor appears between the two attractors, the following conclusions are obtained.

1. When the time parameter t moves from $-\infty$ to $+\infty$, the system will evolve the state of the system completely and sequentially with 10 unit times as a cycle.

2. The change rule of the system and the change rule of the value of $s = \sin(x)$ are synchronized, but they are not a one-to-one correspondence. Different values of $s = \sin(x)$ will not affect the results, but it will make the system evolve its existing state when it changes.

TABLE 2. The value of s and the state of the new system at different time parameter t values.

t	s	Status	t	s	Status
-30	0	Chaos	0	0	Chaos
-29	-0.9511	Period(left)	1	-0.9511	Period(left)
-28	0.5878	Period(right)	2	0.5878	Period(right)
-27	0.5878	Chaos	3	0.5878	Chaos
-26	-0.9511	Period(right)	4	-0.9511	Period(right)
-25	0	Period(right)	5	0	Period(right)
-24	0.9511	Period(right)	6	0.9511	Period(right)
-23	-0.5878	Chaos	7	-0.5878	Chaos
-22	-0.5878	Period(left)	8	-0.5878	Period(left)
-21	0.9511	Period(right)	9	0.9511	Period(right)
-20	0	Chaos	10	0	Chaos
-19	-0.9511	Period(left)	11	-0.9511	Period(left)
-18	0.5878	Period(right)	12	0.5878	Period(right)
-17	0.5878	Chaos	13	0.5878	Chaos
-16	-0.9511	Period(right)	14	-0.9511	Period(right)
-15	0	Period(right)	15	0	Period(right)
-14	0.9511	Period(right)	16	0.9511	Period(right)
-13	-0.5878	Chaos	17	-0.5878	Chaos
-12	-0.5878	Period(left)	18	-0.5878	Period(left)
-11	0.9511	Period(right)	19	0.9511	Period(right)
-10	0	Chaos	20	0	Chaos
-9	-0.9511	Period(left)	21	-0.9511	Period(left)
-8	0.5878	Period(right)	22	0.5878	Period(right)
-7	0.5878	Chaos	23	0.5878	Chaos
-6	-0.9511	Period(right)	24	-0.9511	Period(right)
-5	0	Period(right)	25	0	Period(right)
-4	0.9511	Period(right)	26	0.9511	Period(right)
-3	-0.5878	Chaos	27	-0.5878	Chaos
-2	-0.5878	Period(left)	28	-0.5878	Period(left)
-1	0.9511	Period(right)	29	0.9511	Period(right)
			30	0	Chaos

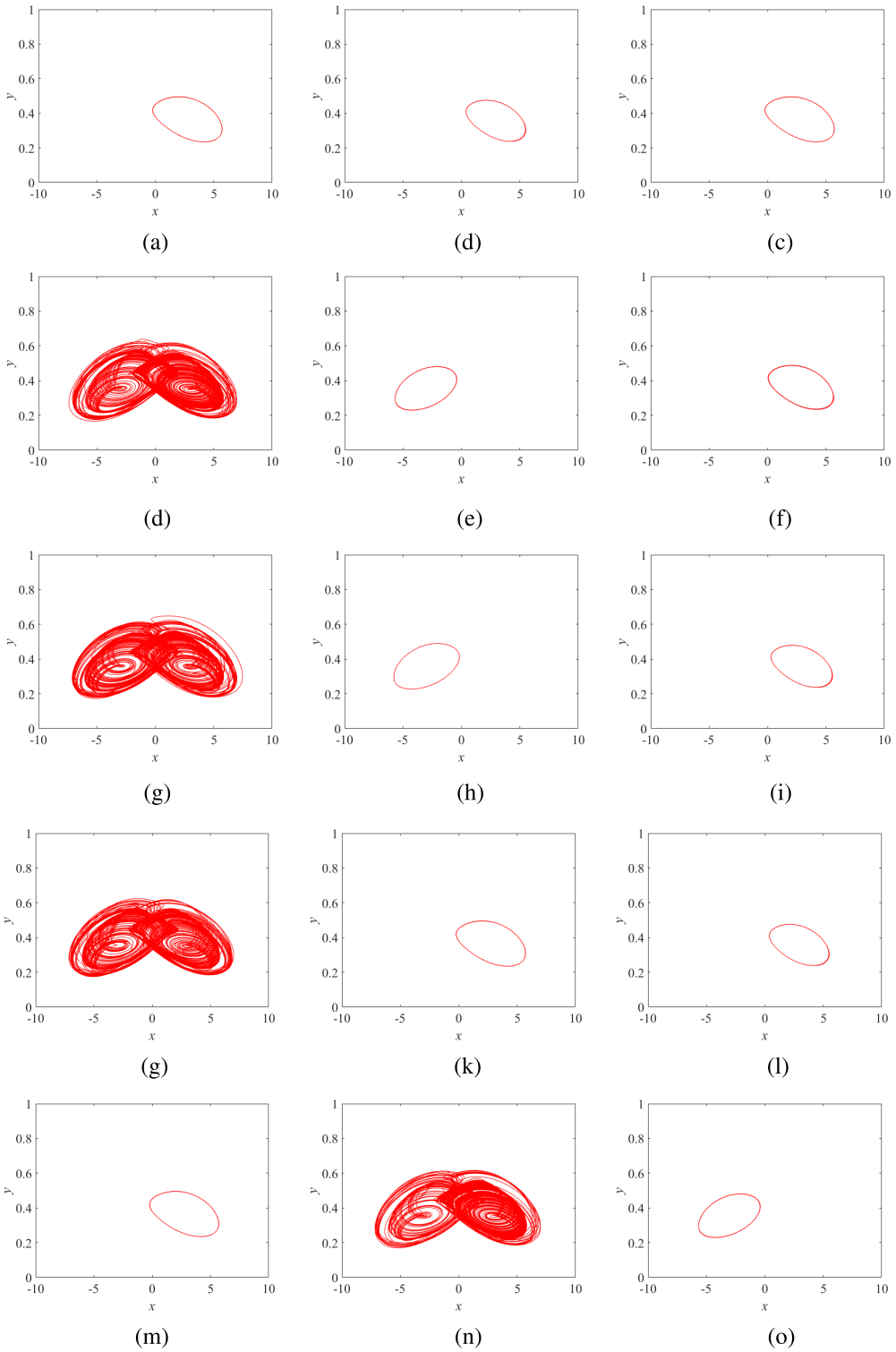

FIGURE 10. When the new system parameters are $a = 55$, $b = 167$, $c = 6.9$, $A = 19$, $f = 5.7$, and the initial value is (10, 0, 3), the chaotic attractor of the x-y plane with different time parameters t, (a) $t = 4$, (b) $t = 5$, (c) $t = 6$, (d) $t = 7$, (e) $t = 8$, (f) $t = 9$, (g) $t = 10$, (h) $t = 11$, (i) $t = 12$, (j) $t = 13$, (k) $t = 14$, (l) $t = 15$, (m) $t = 16$, (n) $t = 17$, (o) $t = 18$.

3. The time parameter t value will not change the nature of the system. It will not make a non-chaotic system into chaos.

4. As the value of the time parameter t becomes more and more accurate, the state transition of the system will become more and more detailed, and even a periodic state between the limit cycle and chaos will appear.

The change rule of the system and the change rule of the value of $s = \sin(x)$ are synchronized, but they are not a one-to-one correspondence.

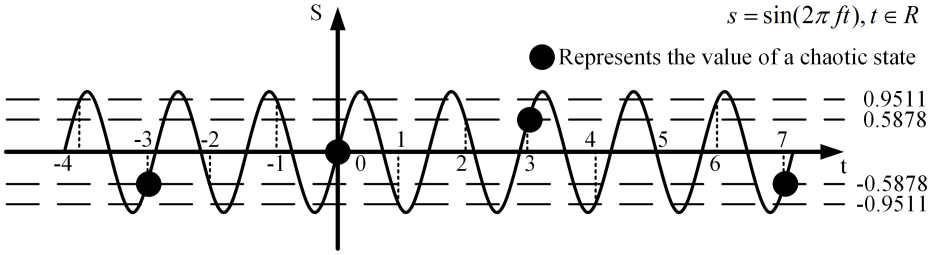

FIGURE 11. Schematic diagram of the relationship between the value of *s* and the new system state at different time parameters *t*.

TABLE 3. The value of *s* and the state of the new system at different time parameter *t* values.

t	*s*	Status	*t*	*s*	Status
3.0	0.5878	Chaos	5.1	0.4258	Chaos
3.1	-0.8763	Period(left)	5.2	-0.7705	Period(left)
3.2	0.9980	Period(right)	5.3	0.9686	Period(right)
3.3	-0.9298	Period(right)	5.4	-0.9823	Period(left)
3.4	0.6845	Period(right)	5.5	0.8090	Period(right)
3.5	-0.3090	Chaos	5.6	-0.4818	Chaos
3.6	-0.1253	Period(right)	5.7	0.0628	Period(right)
3.7	0.5358	Chaos	5.8	0.3681	Chaos
3.8	-0.8443	Period(left)	5.9	-0.7290	Period(left)
3.9	0.9921	Period(right)	6.0	0.9511	Period(right)
4.0	0.9511	Period(right)	6.1	-0.9921	Period(left)
4.1	0.7290	Period(right)	6.2	0.8443	Period(right)
4.2	-0.3681	Chaos	6.3	-0.5358	Chaos
4.3	-0.0628	Period(right)	6.4	0.1253	Period(right)
4.4	0.4818	Chaos	6.5	0.3090	Chaos
4.5	-0.8090	Period(left)	6.6	-0.6845	Period(left)
4.6	0.9823	Period(right)	6.7	0.9298	Period(right)
4.7	-0.9686	Period(left)	6.8	-0.9980	Period(left)
4.8	0.7705	Period(right)	6.9	0.8763	Period(right)
4.9	-0.4258	Chaos	7.0	-0.5878	Chaos
5.0	0	Period(right)	7.1	0.1874	Period(right)

To verify the above conjecture, the chaotic state of the system is predicted. When the system parameters are selected as $a = 55$, $b = 167$, $c = 6.9$, $A = 19$, $f = 5.7$, and the initial value is (10, 0, 3). According to the laws of the system, when $t = 107$, the system should be in chaos, when $t = 28.4$, the system should be in chaos, and when $t = 15.18$, the system should be in a period. The attractor of the *x*-*y* plane is shown in Fig. 12.

From Fig. 12 and the above experimental data, the periodic coexistence attractor is consistent with the above five conclusions, and the analysis of this special phenomenon is completely reliable.

IV. ACTUAL ANALOG CIRCUIT RESULTS

A. PHYSICAL CIRCUIT DESIGN AND PARAMETER SELECTION

The new system defined by Eq. (6) should be implemented for easy using. Design the main circuit, memristor main circuit, and absolute value circuit by using operational

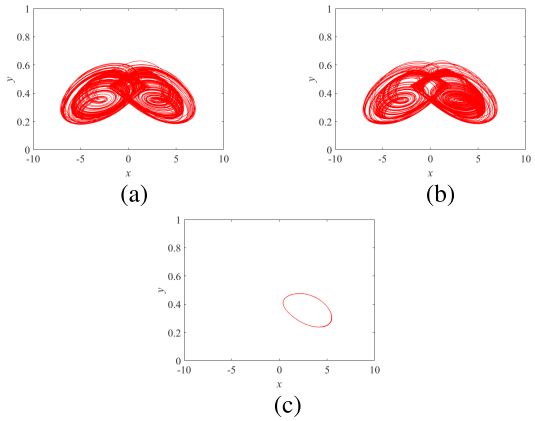

FIGURE 12. When the new system parameters are $a = 55$, $b = 167$, $c = 6.9$, $A = 19$, $f = 5.7$, and the initial value is (10, 0, 3), the predicted chaotic attractor of the *x*-*y* plane with different time parameters *t*, (a) $t = 107$, (b) $t = 28.4$, (c) $t = 15.18$.

amplifiers, resistors, capacitors, diodes, and multipliers. The circuit schematic diagram is shown in Fig. 13.

The ideal magnetron memristor consists of a voltage follower, an inverting integrator, an absolute value circuit F($f(x) = |x|$), a multiplier and a resistance Rm_2, The mathematical model of the memristor can be easily obtained by analyzing the relationship between the input voltage *vs* and the output current *i*, which is expressed as

$$\begin{cases} i = W(v_z)v_s = \dfrac{g_1}{R_{m2}C_0}v_z v_s = \dfrac{1}{R_{m1}C_0}k v_z v_s \\ \dot{v}_z = \dfrac{1}{R_{m1}C_0}v_s \end{cases} \tag{10}$$

where *vz* is the internal variable of the ideal magnetron memristor, g_1 is the output gain of the multiplier A_1, where $k = g_1 Rm_1/Rm_2$ and $W\ (vz) = kvz/Rm_1C_0$. The main circuit of the new system is composed of two interconnected arithmetic circuits, corresponding to the first and the second differential equation in Eq. (6). According to Kirchhoff?s circuit law and the electrical characteristics of circuit components, the circuit equation of the system is derived, which is expressed as

$$\begin{cases} RC_1\dfrac{dV_x}{dt} = -\dfrac{R}{R_1}V_x + \dfrac{Rg_4R_4}{R_2R_3}V_xV_y - \dfrac{C_1Rg_1}{R_{m2}C_0}|V_z|\,V_s \\ RC_2\dfrac{dV_y}{dt} = -\dfrac{R}{R_5}V_y - \dfrac{R}{R_6}V_y - \dfrac{Rg_2g_3}{R_8}{V_x}^2V_y - \dfrac{R}{R_7}V \\ RC_0\dfrac{dV_z}{dt} = \dfrac{R}{R_{m1}}V_s \end{cases} \tag{11}$$

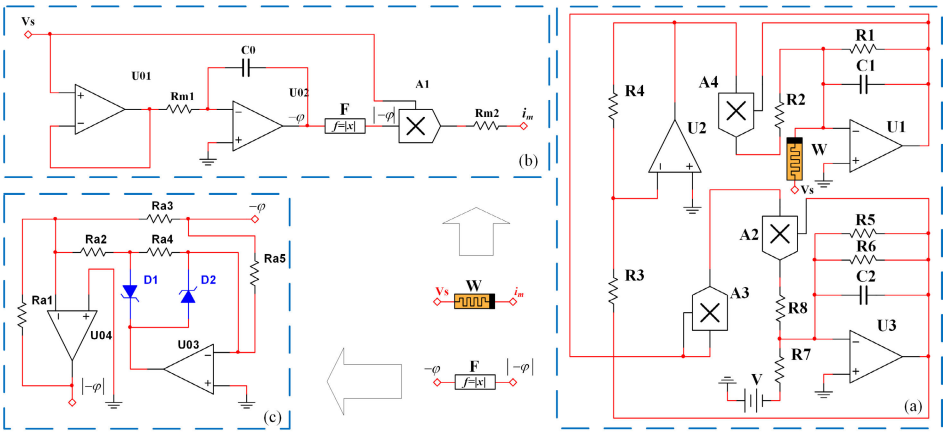

FIGURE 13. Schematic diagram of the circuit of the EDFL, (a) Main circuit of EDFL, (b) Main circuit of the ideal magnetron memristor, (c) Absolute value circuit.

where vx, vy, and vz are three circuit variables, V is a DC voltage source, vs is an ideal AC voltage source input to the magnetron memristor, and g_1, g_2, g_3 and g_4 are the gains of multipliers A_1, A_2, A_3 and A_4. By comparing Eq. (6) and Eq. (11), the proportional relationship between the resistances is obtained, which is expressed as

$$\begin{cases} R_{m2} = g_1 R_{m1} \\ R_1 = \dfrac{R_{m1}}{a} \\ R_2 = \dfrac{g_4 R_4 R_{m1}}{R_3 R_3 b} \\ R_5 = R_{m1} \\ R_6 = \dfrac{R_{m1}}{c} \\ R_7 = R_{m1} \\ R_8 = g_2 g_3 R_{m1} \end{cases} \tag{12}$$

Let the Scaling factor $\tau = 1000\mu s$, that is, $R = 50\text{K}\Omega$ and $C = 20\text{nF}$. According to Eq. (10) and Eq. (11), the numerical information of the circuit components that can be used for actual circuit welding is obtained, as shown in Table 4 Shown.

B. CIRCUIT SIMULATION AND ACTUAL CIRCUIT EXPERIMENTN

According to the circuit design above, the phase diagram from Multisim numerical simulation are shown in Fig. 14.

According to the circuit parameters in Fig. 13 and Table 4, an actual circuit soldered with electronic components can be implemented on a breadboard. The operational amplifier AD711JN and the multiplier AD633JN powered by ±15V DC power are selected and the diode is selected as the 1N4148 model. The voltage source is UTG6000B series arbitrary waveform generator produced by Uni-Trend Technology Limited, and the result is displayed on UTD7102H digital oscilloscope produced by Uni-Trend Technology Limited. The actual photo of the new system model is shown in Fig. 15, and the functional modules of the circuit are shown in Table 5.

TABLE 4. Circuit parameters of Eq. (11) for simulations.

Parameters	Components	Values
R_1	Resistance	0.9KΩ
R_2	Resistance	0.3KΩ
R_3,R_4	Resistance	10KΩ
R_5,R_7,R_8	Resistance	50 KΩ
R_6	Resistance	7.2KΩ
A_2,A_3,A_4	Multiplier gain	1
C_1,C_2	Capacitance	20nF
V	DC voltage	5.9V
Rm_1	Resistance	50KΩ
Rm_2	Resistance	69KΩ
C_0	Capacitance	20nF
A_1	Multiplier gain	1
R_1,R_3,R_4	Resistance	10KΩ
R_2	Resistance	5KΩ
R_1	Resistance	10KΩ

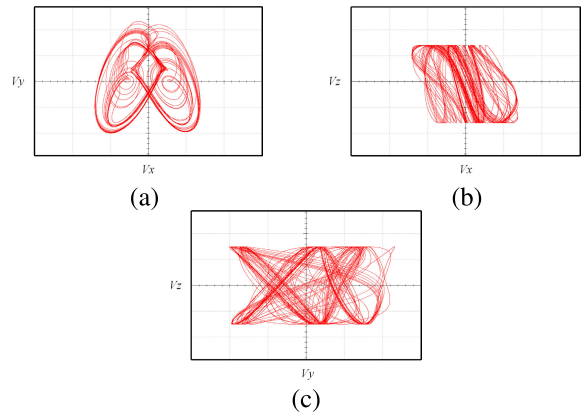

FIGURE 14. When the component values are shown in Table 4, the numerical simulation phase diagram of the new system on multisim, (a) *x-y* plane, (b) *x-z* plane, (c) *y-z* plane.

When vz is set to $vz = 2\text{V}$, $vz = 3\text{V}$, $vz = 6\text{V}$ and $vz = 7$ V, respectively, the vx-vy plane phase diagrams are shown in Fig. 16. The experimental results show that in the

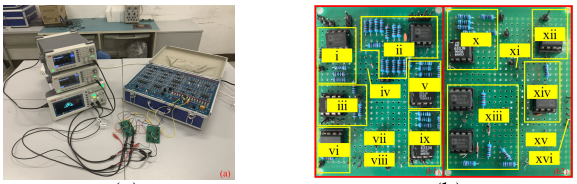

(a) (b)

FIGURE 15. Photograph of the experimental prototype, (a) Hardware breadboard, (b1) Experimental circuit of memristor, (b2) Experimental circuit of the main circuit.

TABLE 5. Circuit parameters of Eq. (11) for simulations.

Serial number	Function	Values
i	Integrator	/
ii	Integrator	/
iii	Multiplier	1
iv	DC power supply	-15V
v	Multiplier	1
vi	Phase inverter	/
vii	DC power supply	+15V
viii	GND	/
ix	Multiplier	1
x	Multiplier	1
xi	GND	/
xii	Voltage follower	/
xiii	Absolute value	/
xiv	Integrator	/
xv	DC power supply	-15V
xvi	DC power supply	+15V

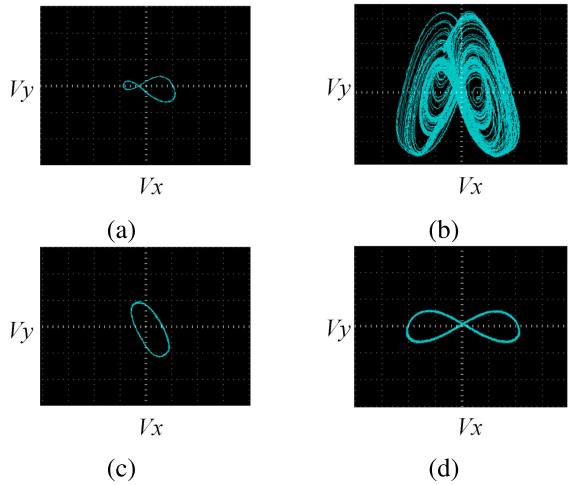

FIGURE 16. Experiments have measured the symmetrical attractors coexisting with different *vz*. (a) $vz = 2V$, (b) $vz = 3V$, (c) $vz = 6V$, (d) $vz = 7V$.

hard-ware experiment of the new system with memristor, coexisting symmetric attractors can also be obtained.

V. CONCLUSION

In the paper, a new memristor laser chaotic system was proposed. The memristor and sinusoidal AC voltage were introduced into the laser systems by modulation method. In this way, the EDFL was transformed into a third-order non-autonomous memristor laser chaotic system. Numerical analysis results show that the new system has two different types of attractor coexistence phenomena, one is the coexistence of symmetrical attractors, and the other is the coexistence of periodic attractors, and both of them coexist in periodic and chaotic states. In the phenomenon of periodic attractor coexistence, the system can evolve from the period to other states between chaos, and this evolution is controllable and regular, that is, the phase diagram of the corresponding state of the system can be accurately obtained by changing the value of the time parameter of the AC power supply. Besides, a simulation circuit was designed according to the system equation, and the initial value of the system was changed by repeatedly turning on the power. The results of the oscilloscope show that the actual circuit and the theoretical analysis had the same dynamical characteristics, and both had the special attractor coexistence phenomenon. The new system is achievable and has broad application prospects in information encryption and secure communication, because of its special attractor coexistence phenomenon and extremely complex dynamic characteristics. Next, we will explore more practical applications of this new system.

REFERENCES

[1] C. O. Weiss and W. Klische, "On observability of lorenz instabilities in lasers," *Opt. Commun.*, vol. 51, no. 1, pp. 47–48, Aug. 1984.
[2] C. O. Weiss, W. Klische, P. S. Ering, and M. Cooper, "Instabilities and chaos of a single mode NH3 ring laser," *Opt. Commun.*, vol. 52, no. 6, pp. 405–408, Jan. 1985.
[3] P. Mandel, "Influence of Doppler broadening on the stability of monomode ring lasers," *Opt. Commun.*, vol. 44, no. 6, pp. 400–404, Feb. 1983.
[4] L. Casperson, "Spontaneous coherent pulsations in ring-laser oscillators: Simplified models," *IEEE J. Quantum Electron.*, vol. 14, no. 10, pp. 756–761, Jan. 2003.
[5] N. J. Halas, S.-N. Liu, and N. B. Abraham, "Route to mode locking in a three-mode He-Ne 3.39–μm laser including chaos in the secondary beat frequency," *Phys. Rev. A, Gen. Phys.*, vol. 28, no. 5, pp. 2915–2920, Nov. 1983.
[6] S. Yan, "All-optical chaotic MQW laser repeater for long-haul chaotic communications," *Chin. Opt. Lett.*, vol. 3, no. 5, pp. 283–286, 2005.
[7] S. Yan, Z. Chi, and W. Chen, "Chaotic laser synchronization and its application in optical fiber secure communication," *Sci. China*, vol. 47, no. 3, pp. 332–347, 2004.
[8] S. Yan, "Enhancement of chaotic carrier bandwidth in a semiconductor laser transmitter using self-phase modulation in an optical fiber external round cavity," *Chin. Sci. Bull.*, vol. 55, no. 11, pp. 1007–1012, Apr. 2010.
[9] S. Ali, K. Alkhateeb, and B. Bouzid, "A novel erbium-doped fiber laser source (EDFL)," in *Proc. Int. Conf. Comput. Commun. Eng.*, 2008, pp. 538–541.
[10] X. Bai, C. Mou, L. Xu, S. Huang, T. Wang, S. Pu, and X. Zeng, "Passively Q-switched EDFL using Fe_3O_4-nanoparticle saturable absorber," 2015, *arXiv:1511.07016*. [Online]. Available: https://arxiv.org/abs/1511.07016
[11] J. Chow, G. Town, B. Eggleton, M. Ibsen, K. Sugden, and I. Bennion, "Multiwavelength operation of an erbium-doped fiber laser by using in-fiber comb filters," in *Conf. Lasers Electro-Opt., OSA Tech. Dig.*, vol. 15. Optical Society of America, May 1995, Paper CMB6.
[12] C. R. Giles and E. Desurvire, "Modeling erbium-doped fiber amplifiers," *J. Lightw. Technol.*, vol. 9, no. 2, pp. 271–283, Feb. 1991.
[13] R. J. Mears, L. Reekie, I. M. Jauncey, and D. N. Payne, "Low-noise erbium-doped fibre amplifier operating at 1.54 μm," *Electron. Lett.*, vol. 23, no. 19, pp. 1026–1028, 1987.
[14] F. Sanchez, M. LeFlohic, G. M. Stephan, P. LeBoudec, and P.-L. Francois, "Quasi-periodic route to chaos in erbium-doped fiber laser," *IEEE J. Quantum Electron.*, vol. 31, no. 3, pp. 481–488, Mar. 1995.

[15] G. D. Vanwiggeren and R. Roy, "Communication with chaotic lasers," *Science*, vol. 279, no. 5354, pp. 1198–1200, 1998.

[16] F. Wu, J. Li, Z. Yuebin, W. Xiaoming, and Z. Kaixuan, "Dual-ring erbium-doped fiber laser chaos controlled by coupling feedback phase-shift," \emphInfr. Laser Eng., vol. 41, no. 4, pp. 895–900, 2012.

[17] T. B. Mork and J. Mark, *Chaos in Semiconductor Lasers With Optical Feedback*. Boston, MA, USA: Springer, 1993.

[18] F. T. Arecchi, R. Meucci, and L. Pezzati, "Chaos in a CO_2 waveguide laser due to transverse-mode competition," *Phys. Rev. A, Gen. Phys.*, vol. 42, no. 9, pp. 5791–5793, Nov. 1990.

[19] S. Z. Ali, M. K. Islam, and M. Zafrullah, "Effect of parametric variation on generation and enhancement of chaos in erbium-doped fiber-ring lasers," *Opt. Eng.*, vol. 49, no. 10, p. 730, 2010.

[20] F. Zhang and P. L. Chu, "Effect of transmission fiber on chaos communication system based on erbium-doped fiber ring laser," *J. Lightw. Technol.*, vol. 21, no. 12, pp. 3334–3343, Dec. 2003.

[21] F. Chang, F. Yu-Ling, Y. Zhi-Hai, F. Jian, S. Yuan-Chao, and Z. Yu-Zhu, "Experimental investigation on chaos generation in erbium-doped fiber single-ring lasers," *Chin. Phys. B*, vol. 21, no. 10, pp. 155–158, 2012.

[22] M. Sciamanna and K. A. Shore, "Physics and applications of laser diode chaos," *Nature Photon.*, vol. 9, no. 3, pp. 151–162, Mar. 2015.

[23] G. Aromataris and V. Annovazzi-Lodi, "Two- and three-laser chaos communications," in *Proc. 18th Italian Nat. Conf. Photonic Technol.*, 2016, pp. 1–4.

[24] F. Yu, L. Liu, H. Shen, Z. Zhang, Y. Huang, C. Shi, S. Cai, X. Wu, S. Du, and Q. Wan, "Dynamic analysis, circuit design, and synchronization of a novel 6D memristive four-wing hyperchaotic system with multiple coexisting attractors," *Complexity*, vol. 2020, pp. 1–17, May 2020.

[25] L. Chua, "Memristor—The missing circuit element," *IEEE Trans. Circuit Theory*, vol. CT-18, no. 5, pp. 507–519, Sep. 1971.

[26] L. O. Chua and S. M. Kang, "Memristive devices and systems," *Proc. IEEE*, vol. 64, no. 2, pp. 209–223, Feb. 1976.

[27] S. P. Adhikari, M. P. Sah, H. Kim, and L. O. Chua, "Three fingerprints of memristor," *IEEE Trans. Circuits Syst. I, Reg. Papers*, vol. 60, no. 11, pp. 3008–3021, Nov. 2013.

[28] S. Singh, P. W. C. Prasad, A. Alsadoon, A. Beg, L. Pham, and A. Elchouemi, "Survey on memrister models," in *Proc. Int. Conf. Electron., Inf., Commun. (ICEIC)*, 2016, pp. 1–7.

[29] J. Sun, G. Han, and Z. Zeng, "Memristor-based neural network circuit of full-function pavlov associative memory with time delay and variable learning rate," *IEEE Trans. Cybern.*, vol. 50, no. 7, pp. 2935–2945, Nov. 2019.

[30] Z. Xu, Z. Yu-Ze, B. Qiang, Y. Xing-Hua, and Z. Yun-Xiao, "The mathematical model and properties of memristor with border constraint," *Acta Phys. Sinica*, vol. 59, no. 9, p. 6673, 2010.

[31] X. Chen, C. Feng, Z. L. Wu, F. Yang, Y. Liu, S. Jiang, M. H. Li, and G. H. Yu, "Interfacial oxygen migration and its effect on the magnetic anisotropy in Pt/Co/MgO/Pt films," *Appl. Phys. Lett.*, vol. 104, no. 5, p. 3515, 2014.

[32] C. Jiang, C. Zhang, C. Dong, D. Guo, and D. Xue, "Electric field tuning of non-volatile three-state magnetoelectric memory in FeCo-$NiFe_2O_4$/$Pb(Mg_{1/3}Nb_{2/3})_{0.7}Ti_{0.3}O_3$ heterostructures," *Appl. Phys. Lett.*, vol. 106, no. 12, Mar. 2015, Art. no. 122406.

[33] F. Yu, S. Qian, X. Chen, Y. Huang, L. Liu, C. Shi, S. Cai, Y. Song, and C. Wang, "A new 4D four-wing memristive hyperchaotic system: Dynamical analysis, electronic circuit design, shape synchronization and secure communication," *Int. J. Bifurcation Chaos*, vol. 30, no. 10, Aug. 2020, Art. no. 2050147.

[34] Y.-H. Chu, L. W. Martin, M. B. Holcomb, M. Gajek, S.-J. Han, Q. He, N. Balke, C.-H. Yang, D. Lee, W. Hu, Q. Zhan, P.-L. Yang, A. Fraile-Rodríguez, A. Scholl, S. X. Wang, and R. Ramesh, "Electric-field control of local ferromagnetism using a magnetoelectric multiferroic," *Nature Mater.*, vol. 7, no. 6, pp. 478–482, Jun. 2008.

[35] Y. Imai, H. Murakawa, and T. Imoto, "Chaos synchronization characteristics in erbium-doped fiber laser systems," *Opt. Commun.*, vol. 217, nos. 1–6, pp. 415–420, Mar. 2003.

[36] S. Kim, B. Lee, and D. H. Kim, "Experiments on chaos synchronization in two separate erbium-doped fiber lasers," *IEEE Photon. Technol. Lett.*, vol. 13, no. 4, pp. 290–292, Apr. 2001.

[37] M. K. Abd-Rahman, S. Selvakennedy, P. Poopalan, and H. Ahmad, "Operating wavelength of erbium-doped fiber-ring laser," *Microw. Opt. Technol. Lett.*, vol. 31, no. 2, pp. 105–107, 2001.

[38] B. Tang, J. Lin, and J. Bai, "The innovation of multi-wavelength erbium-doped fiber laser," in *Proc. Int. Conf. Softw. Eng. Service Sci.*, 2015, pp. 920–922.

[39] K. M. Manfred, L. Ciaffoni, and G. A. D. Ritchie, "Optical-feedback cavity-enhanced absorption spectroscopy in a linear cavity: Model and experiments," *Appl. Phys. B, Lasers Opt.*, vol. 120, no. 2, pp. 329–339, Aug. 2015.

[40] H. Shimizu, S. Araki, Y. Funahashi, Y. Honda, T. Okugi, T. Omori, N. Terunuma, J. Urakawa, M. Kuriki, S. Miyoshi, and T. Takahashi, "Photon generation by laser-Compton scattering using an optical resonant cavity at the KEK-ATF electron ring," *J. Phys. Soc. Jpn.*, vol. 78, no. 7, p. 4501, 2011.

[41] D. D. Holm, G. Kovačič, and T. A. Wettergren, "Near-integrability and chaos in a resonant-cavity laser model," *Phys. Lett. A*, vol. 200, nos. 3–4, pp. 299–307, Apr. 1995.

[42] T. Georges, C. Chauzat, A. Poivre, N. Landru, and J. Rouvillain, "Short and long term frequency stability of linear monolithic intra-cavity frequency-doubled solid-state laser," *Proc SPIE*, vol. 7578, Feb. 2010, Art. no. 75780U.

[43] F. Amini, M. Fathipour, and A. Haghparast, "Comparison between different graded non-resonant cavity in blue laser diodes," in *Proc. 1st Asian Conf. Appl. Electromagn. Wave Opt., Comput. Electromagn.*, 2012, pp. 1–4.

[44] B. Romeira, J. M. L. Figueiredo, T. J. Slight, L. Wang, E. Wasige, and C. N. Ironside, "Wireless to optical frequency locking and chaos using a resonant tunnelling-laser diode circuit," in *Proc. IEEE/LEOS Winter Topicals Meeting Series*, Jan. 2009, pp. 128–129.

[45] K. B. Shaik and M. K. Mandal, "Chaos from jerk circuit," *Resonance*, vol. 15, no. 3, pp. 257–267, Mar. 2010.

[46] J. Sun, Y. Wu, G. Cui, and Y. Wang, "Finite-time real combination synchronization of three complex-variable chaotic systems with unknown parameters via sliding mode control," *Nonlinear Dyn.*, vol. 88, no. 3, pp. 1677–1690, May 2017.

[47] K. Murali, M. Lakshmanan, and L. O. Chua, "Bifurcation and chaos in the simplest dissipative non-autonomous circuit," *Int. J. Bifurcation Chaos*, vol. 4, no. 6, pp. 1511–1524, Dec. 1994.

[48] X. Fan Wang, G.-Q. Zhong, K.-S. Tang, K. F. Man, and Z.-F. Liu, "Generating chaos in Chua's circuit via time-delay feedback," *IEEE Trans. Circuits Syst. I, Fundam. Theory Appl.*, vol. 48, no. 9, pp. 1151–1156, Sep. 2001.

[49] P. Besnard, F. Ginovart, P. Le Boudec, F. Sanchez, and G. M. Stéphan, "Experimental and theoretical study of bifurcation diagrams of a dual-wavelength erbium-doped fiber laser," *Opt. Commun.*, vol. 205, nos. 1–3, pp. 187–195, Apr. 2002.

[50] A. N. Pisarchik and Y. O. Barmenkov, "Locking of self-oscillation frequency by pump modulation in an erbium-doped fiber laser," *Opt. Commun.*, vol. 254, nos. 1–3, pp. 128–137, Oct. 2005.

[51] X.-P. Zheng, X.-J. Tian, and F. Zheng, "Research on image encryption based on erbium-doped fiber laser system with optical delay feedback," *J. China Universities Posts Telecommun.*, vol. 16, pp. 74–77, Sep. 2009.

[52] B. C. Bao, J. P. Xu, and Z. Liu, "Initial state dependent dynamical behaviors in a memristor based chaotic circuit," *Chin. Phys. Lett.*, vol. 27, no. 7, pp. 51–53, 2010.

[53] B.-C. Bao, X. Jian-Ping, Z. Guo-Hua, M. Zheng-Hua, and Z. Ling, "Chaotic memristive circuit: Equivalent circuit realization and dynamical analysis," *Chin. Phys. B*, vol. 20, no. 12, pp. 109–115, 2011.

[54] J. Sun, X. Zhao, J. Fang, and Y. Wang, "Autonomous memristor chaotic systems of infinite chaotic attractors and circuitry realization," *Nonlinear Dyn.*, vol. 94, no. 4, pp. 2879–2887, Dec. 2018.

[55] F. Yang, J. Mou, C. Ma, and Y. Cao, "Dynamic analysis of an improper fractional-order laser chaotic system and its image encryption application," *Opt. Lasers Eng.*, vol. 129, Jun. 2020, Art. no. 106031.

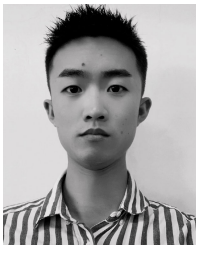

JIEYANG WANG received the B.S. degree from Dalian Polytechnic University, Dalian, China, in 2019, where he is currently pursuing the Ph.D. degree in optical engineering. His research interests include chaos theory and chaos electronic circuits.

HONGJIE LI received the M.S. degree in signal and information processing from the Dalian University of Technology, Dalian, China. She is currently a Lecturer with the School of Information Science and Engineering, Dalian Polytechnic University, China. Her main research interests include the digital image processing, non-gaussian, and non-stationary signal processing theory.

ZHISEN WANG received the B.S. and M.S. degrees from Jilin University, Jilin, China, and the Ph.D. degree in electrical and communication engineering from Tohoku University, Sendai, Japan, in 2007. He is currently a Professor with the School of Information Science and Engineering, Dalian Polytechnic University. His research interests include wireless communication and networks, digital signal processing, and the IoT theory and technology.

JUN MOU received the B.S., M.S., and Ph.D. degrees in physics and electronics from Central South University, Changsha, China. He is currently an Associate Professor with the School of Information Science and Engineering, Dalian Polytechnic University, China. His main research interests include the nonlinear system control, secure communication, power system automation, and smart grid research.